Quantum Electronics **46** (5) 447–450 (2016) ©2016 Kvantovaya Elektronika and Turpion Ltd

LASERS

DOI: 10.1070/QEL16058

Quantum cascade laser based on $GaAs/Al_{0.45}Ga_{0.55}As$ heteropair grown by MOCVD

I.I. Zasavitskii, A.N. Zubov, A.Yu. Andreev, T.A. Bagaev, P.V. Gorlachuk, M.A. Ladugin, A.A. Padalitsa, A.V. Lobintsov, S.M. Sapozhnikov, A.A. Marmalyuk

Abstract. **A pulsed quantum cascade laser emitting in the wavelength range 9.5–9.7 μm at 77.4 K is developed based on the $GaAs/Al_{0.45}Ga_{0.55}As$ heteropair. The laser heterostructure was grown by MOCVD. The threshold current density was 1.8 kA cm^{-2}. The maximum output power of the laser with dimensions of 30 μm × 3 mm and with cleaved mirrors exceeded 200 mW.**

Keywords: *quantum cascade laser, MOCVD, GaAs/AlGaAs heteropair, mid-IR spectral region.*

1. Introduction

Quantum cascade laser (QCLs) is a unipolar device based on intersubband transitions in quantum wells. Mid-IR (3–24 μm) QCLs are developed mainly based on lattice-matched or strained GaInAs/AlInAs/InP heterostructures. However, there exists another heteropair, namely, $GaAs/Al_xGa_{1-x}As$, which is technologically proven and became classical. From the viewpoint of the development of QCLs, this heteropair has two drawbacks. First, it has a relatively small quantum well depth, which is only 0.39 eV at the Al fraction $x = 0.45$. In heteropairs of this composition, the extrema in the conduction band are degenerate and electrons can migrate to the X and L satellite valleys. Thus, the maximum energy of optical transitions in quantum wells does not exceed 0.15 eV, which allows one to obtain radiation with wavelengths of 8 μm and longer. The second drawback of the discussed heteropair is a relatively large effective mass in quantum wells, which decreases the optical gain by approximately two times compared to the GaInAs/AlInAs pair.

However, we should also note advantages of the $GaAs/Al_xGa_{1-x}As$ heteropair. First of all, it has good lattice matching in a wide range of the solid solution composition. In addition, to create a large number of quantum wells (the number of heterojunctions in QCLs exceeds 500) during the growth of the active laser region, it is possible to switch only one precursor (element source), namely, Al, and thus to ensure the heteropair composition stability, which is especially important for QCLs. These advantages to some extent compensate for the above drawbacks and allow one to hope that, based on the $GaAs/Al_xGa_{1-x}As$ heteropair, it will be possible to fabricate QCLs emitting in the practically important spectral range 8–12 μm by commercial MOCVD. Note also that GaAs substrates are much cheaper than InP substrates.

Mid-IR GaAs/AlGaAs QCLs grown by molecular beam epitaxy were demonstrated for the first time in [1]. Later, lasers with noticeably better characteristics were fabricated by the same method in [2–4]. At present, there exist devices operating in pulsed regimes at 300 K [2] and emitting a power up to 1.1 W at 77 K [5]. The lasers also operate in a cw regime at the maximum working temperature reaching 150 K [6].

Laser heterostructures based on the same heteropair were also grown by MOCVD in [7]; to improve optical confinement in QCLs, the authors of [8] used cladding layers of $In_{0.49}Ga_{0.51}P$ solid solution [8].

In the present work, we report a quantum cascade laser based on a $GaAs/Al_{0.45}Ga_{0.55}As$ heteropair, which is grown by MOCVD and emits at a wavelength of 9.5–9.7 μm.

2. Laser heterostructure design

As a working scheme, we chose an active region of three quantum wells, in which a diagonal optical transition is dominant [3]. Figure 1 presents a calculated energy diagram of a QCL based on the $GaAs/Al_{0.45}Ga_{0.55}As$ heteropair. The calculation is performed for the following active region structure: **4.6**/1.9/**1.1**/5.4/**1.1**/4.8/**2.8**/3.4/**1.7**/3.0/**<u>1.8</u>**/<u>2.8</u>/**<u>2.0</u>**/<u>3.0</u>/**2.6**/3.0 [3], in which the thicknesses of epitaxial layers, beginning from the injection barrier, are given in nanometers. Here, the barrier thicknesses are written in bold type, the quantum-well thicknesses are given in ordinary type, and the doped layers are underlined. In calculation, it was assumed that the radiation wavelength lies in the spectral region near 10 μm. In Fig. 1, lines 3 and 2 belong to the working levels between which an optical transition with an energy of 135 meV occurs. Level 1 is spaced from level 2 by 43 meV and serves to depopulate the lower laser level via scattering by longitudinal optical phonons. The closest to the upper laser level is level 4, which is spaced by 68 meV, i.e., lies sufficiently high for laser operation even at room temperature. The injector ground level g lies 15 meV lower than the upper laser level, owing to which the dynamic range of the pump power is sufficiently wide.

In the considered scheme of the active laser region, the wave functions of the states $n = 3$ and $n = 4$ anticross at some

I.I. Zasavitskii, A.N. Zubov P.N. Lebedev Physics Institute, Russian Academy of Sciences, Leninskii prosp. 53, 119991 Moscow, Russia; National Research Nuclear University 'MEPhI', Kashirskoe sh. 31, 115409 Moscow, Russia; e-mail: zasavit@sci.lebedev.ru;
A.Yu. Andreev, T.A. Bagaev, P.V. Gorlachuk, M.A. Ladugin, A.A. Padalitsa, A.V. Lobintsov, S.M. Sapozhnikov OJSC 'M.F. Stel'makh Polyus Research Institute', ul. Vvedenskogo 3, 117342 Moscow, Russia;
A.A. Marmalyuk OJSC 'M.F. Stel'makh Polyus Research Institute', ul. Vvedenskogo 3, 117342 Moscow, Russia; National Research Nuclear University 'MEPhI', Kashirskoe sh. 31, 115409 Moscow, Russia

Received 20 February 2016
Kvantovaya Elektronika **46** (5) 447–450 (2016)
Translated by M.N. Basieva

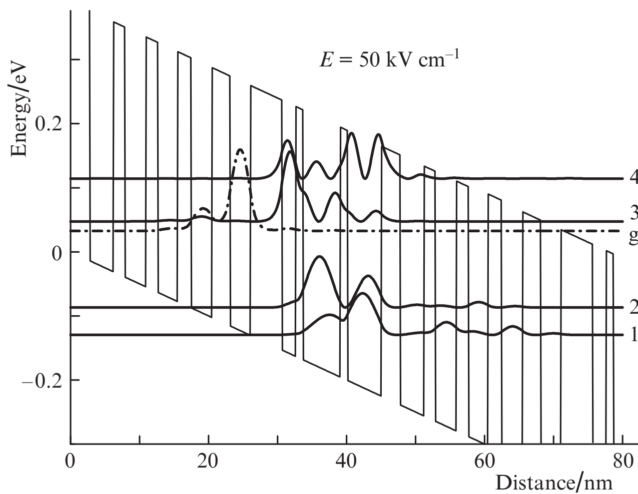

Figure 1. Calculated energy diagram of a QCL based on the GaAs/$Al_{0.45}Ga_{0.55}As$ heteropair. The applied electric field is 50 kV cm^{-1}.

barrier widths and external electric fields and form a doublet with an energy splitting of ~50 meV, which suggests the possibility of a diagonal transition from the first to the second quantum well. The diagonal scheme leads to a decrease in the spatial overlap between the n = 3 and n = 2 states, which decreases the electron–phonon scattering matrix element and increases the lifetime of the state n = 3 (to 1.4 ps [3]) compared to that for the structure with a purely vertical transition. Anticrossing also delocalises the wave function of the n = 3 level to the right-hand neighbouring well, thus increasing its overlap with the wave function of the lower laser level (n = 2) and, therefore, preventing a strong decrease in the dipole matrix element z_{32} (1.7 nm [3]). A drawback of the diagonal scheme is an increase in the number of interfaces due to an additional well in the active region, which leads to a broadening of the luminescence spectrum and, hence, to a lower gain.

For optical confinement, the active region was sandwiched between two GaAs layers with a prescribed doping profile that causes the desired change in the refractive index. In this approach, it is not necessary to use the three-component solid solution AlGaAs; hence, low losses in the waveguide, a weak temperature dependence of these losses, and optimal heat scattering [9] can be achieved. For reliable performance of the waveguide, at this stage of the experiment we also added thin (0.5 μm) heavily doped $Al_{0.2}Ga_{0.8}As$: Si cladding layers. In this case, the molar fraction of AlAs did not exceed x = 0.22 (x ~ 0.3), at which deep levels (DX centres) are formed in the Si-doped solid solution.

3. Growth and study of the laser heterostructure

Laser heterostructures were grown by MOCVD, which was successfully used to form heterostructures with nanometre thicknesses [10–12]. As substrates, we used GaAs (100) doped with Si with concentrations of $(2-3)\times10^{18}$ cm^{-3}. The growth occurred at temperatures of 700–720 °C and pressures of 50–100 mbar.

To create a waveguide, the active region was cladded from both sides by GaAs layers 2.5 m thick with a doping level of 4×10^{16} cm^{-3}, which, in turn, were covered by two $Al_{0.2}Ga_{0.8}As$ (0.5 μm) and GaAs (100–200 nm) layers with an electron concentration of 6×10^{18} cm^{-3}. The δ-doping level in the injector region was $(2-3)\times10^{17}$ cm^{-3}. The active region consisted of 36 cascades.

The X-ray diffraction rocking curve for the individually grown active region of the QCL (Fig. 2) is recorded for the (004) reflection using Cu($K_{\alpha1}$) X-ray radiation. One can see that the active region has a high quality. By the distance between the peaks of the diffraction curve, we calculated the active region period to be 45 nm, which coincides with the expected value.

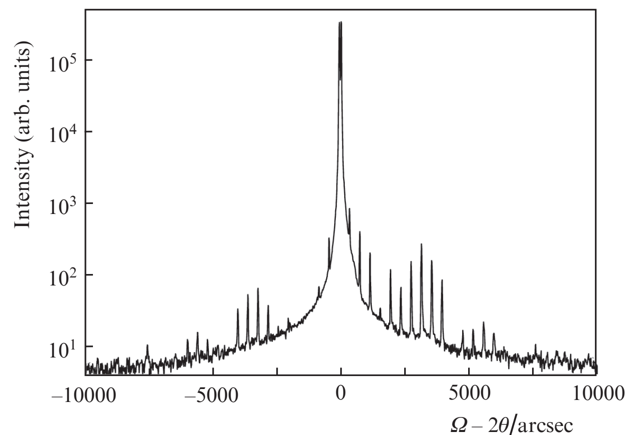

Figure 2. Diffraction curve of a separately grown active region of a QCL recorded for the (004) reflection using the Cu($K_{\alpha1}$) X-ray radiation.

The active region thickness measured on a scanning electron microscope was 1.63 μm. Thus, the calculated thickness of one of the 36 cascades of the active region is 45.3 nm, which agrees with the result obtained from the X-ray diffraction rocking curve analysis.

Figure 3 presents a transmission electron microscopy image of the central part of the active region of the grown heterostructure. One can see that the hetero-interfaces are rather sharp. The thicknesses of the epitaxial layers agree with the values shown in Fig. 1.

The active element was a mesa stripe structure with a mesa width of 30 μm and an etching depth of ~10 μm. The cavity

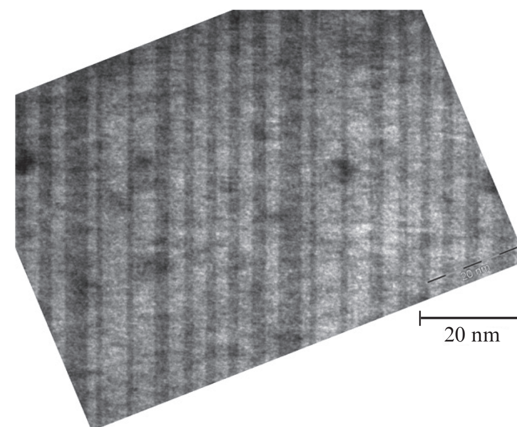

Figure 3. Bright-field transmission electron microscopy image of the central part of the heterostructure active region (GaAs – bright stripes, AlGaAs – dark stripes).

length was 3 mm. Electric insulation was provided by low-temperature plasma-chemical deposition of Si_3N_4 films. For operating at low temperatures, soldering was performed via a Cu–W thermal compensator. The crystal was mounted 'epi-up' on a copper angle-type holder [12].

4. Measurement results and discussion

The threshold current was measured in an optical cryostat at a temperature of 77.4 K. The cold window of the cryostat was made of an antireflection-coated germanium plate. The lasers operated in a pulsed regime (1 μs, 170 Hz). As detectors of integral laser radiation, we used a gold-doped germanium photoresistor or a HgCdTe photodiode. The threshold current was determined from the dependence of the integral radiation intensity on the injection current: as a rule, the radiation intensity was observed to sharply increase (by 2–3 orders of magnitude) near the threshold.

The light–current characteristic of the QCL (Fig. 4) shows that the threshold current is less than 2 A and the multimode emission power is 0.2 W. The average integral radiation power was measured using a VEGA (OPHIR) calorimeter at a pulse repetition rate increased to 1 kHz. To measure low powers inaccessible for the calorimeter, the photodetector and calorimeter signals were matched at a radiation pulse power of about 10 mW. One can see from Fig. 4 that, in the conventional laser geometry, the spontaneous emission region (an expected lower bend of the curve) is hardly achievable.

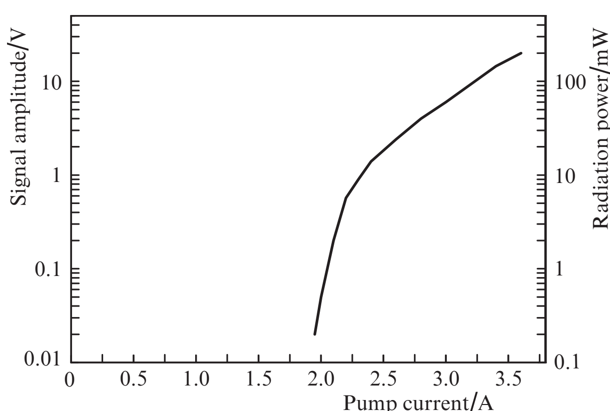

Figure 4. Light–current characteristic of a QCL operating in a pulsed regime (1 μs, 170 Hz) at 77.4 K.

The emission spectra were measured on a Vertex-70 (Bruker) Fourier spectrometer at a temperature of 80 K. KBr plates were used as windows in the cryostat and spectrometer. The Fourier spectrometer operated in the step scan regime and was equipped with a HgCdTe photodiode.

At a current of 3 A, we observed the appearance of a stimulated emission line, whose intensity sharply increases with increasing current. This line corresponds to lasing at one (dominant) longitudinal mode. As a rule, this single-mode regime is retained as the current exceeds the threshold value by approximately 10%.

Multi-mode lasing spectra at different pump currents are shown in Fig. 5. Note that, according to theory, the gain profile at a higher current (7 A) becomes symmetric, and one observes more than 20 equidistant ($\Delta k = 0.49$ cm^{-1}) longitudinal lasing modes. From this, the effective refractive index of

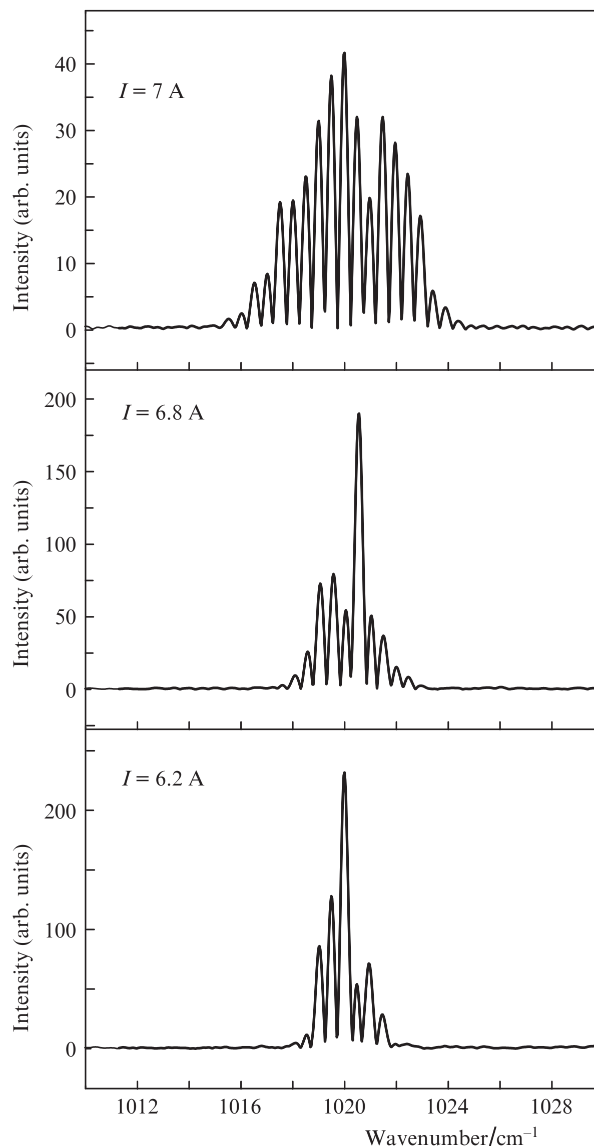

Figure 5. Dependence of the emission spectra of QCL No. 250 on the pump current I at $T = 80$ K, $\tau = 1$ μs.

the laser active media can be estimated as $N_{\rm eff} = 1/(2\Delta kL) = 3.29$, where $L = 3.1$ mm is the cavity length.

The threshold current depended on the growth and post-growth treatment conditions and varied from 2 to 6 A, which corresponded to the threshold current density 2–6 kA cm^{-2}.

Let us estimate the threshold current density of a QCL in the low-temperature approximation by the formula [13]

$$I_{\rm th} = \frac{\varepsilon_0 \lambda N_{\rm eff} L_{\rm p} \Delta E}{4\pi e z_{32}^2} \frac{\alpha_{\rm w} + \alpha_m}{\Gamma \tau_3 (1 - \tau_2/\tau_{32})}.$$

Here, the radiation wavelength is $\lambda = 9.6$ μm, the dipole moment matrix element is $z_{32} = 1.7$ nm [3], the length of the period (cascade) in the active region is $L_{\rm p} = 45$ nm, the cavity length is $L = 3.1$ mm, $N_{\rm eff} = 3.29$, the mirror losses are $\alpha_{\rm m} = 4.2$ cm^{-1}, the waveguide losses measured for two cavity lengths are $\alpha_{\rm w} = 19$ cm^{-1}, the optical confinement factor is $\Gamma = 0.28$, and the spontaneous emission linewidth measured at liquid nitrogen temperature is $\Delta E = 13$ meV. The factor $\tau_3(1 - \tau_2/\tau_{32})$ is about 1 ps [1, 3]. At these parameters, we obtain $I_{\rm th} =$

1.4 kA cm^{-2} at 77.4 K, which is somewhat lower than 1.8–1.9 kA cm^{-2} measured for the best samples. First of all, this points to a good quality of the laser heterostructure grown by MOCVD.

However, as temperature increases from 77 to 205 K, the threshold current density sharply increases, which corresponds to the rather low characteristic temperature T_0 (135 K). For lasers of the same composition ($x = 0.45$) fabricated by molecular-beam epitaxy [3], we estimate the characteristic temperature to be higher and equal to 160 K. The stronger temperature dependence of the threshold current density for our samples cannot be explained by electron transition from the upper laser level $n = 3$ to the high-lying state $n = 4$ or by electron back-transition from the ground (Fermi) level of the injector to the lower laser level $n = 2$. Indeed, according to the calculated energy diagram, the energy gap $E_4 - E_3$ is 60 meV, while the gap $E_2 - E_g$ is 75 meV, which is sufficient for laser operation even at room temperature. One of the reasons for the sharp temperature dependence of the threshold current for our lasers is their low efficiency (below 0.5% at 77 K), which leads to a strong heating of the active region. This is also confirmed by the fact that the threshold current strongly increases as the pulse duration changes from 0.5 to 3 μs. The laser design requires additional optimisation.

Depending on the growth conditions, the laser wavelength varied within the range 9.5–9.7 μm and always exceeded the theoretical value (9.2 μm). One of the reasons for this situation can be slight blurring of the hetero-interfaces in the heterostructure, although, in the first approximation, the heterostructure parameters measured by transmission electron microscopy well agree with the calculated data.

Thus, multi-periodic quantum-well laser heterostructures based on the GaAs/AlGaAs heteropair are grown by MOCVD and quantum cascade lasers for the spectral region near 10 μm are created. QCLs were obtained by a similar method only in [8, 14]. The lasers operated in a pulsed regime (1 μs, 170 Hz) at liquid nitrogen temperature. Typical threshold current densities were 2–4 kA cm^{-2}, the achieved radiation power exceeded 0.2 W, the maximum working temperature was 205 K. By improving the interface quality in the active region of the heterostructure, it will be possible to additionally decrease the threshold current and increase the working temperature of QCLs.

Acknowledgements. The authors thank S.S. Zarubin for the electron microscope measurements. The work of I.I. Zasavitskii and A.N. Zubov was supported by the Russian Academy of Sciences (Programme Nos I.П25 and IV.2.6).

References

1. Sirtori C., Kruck P., Barbieri S., Collot P., Nagle J., Beck M., Faist J., Oesterle U. *Appl. Phys. Lett*., **73**, 3486 (1998).
2. Strasser G., Gianordoli S., Hvozdara L., Schrenk W., Unterrainer K., Gornik E. *Appl. Phys. Lett*., **75**, 1345 (1999).
3. Page H., Becker C., Robertson A., Glastre G., Ortiz V., Sirtori C. *Appl. Phys. Lett*., **78**, 3529 (2001).
4. Liu J-Q., Liu F-Q., Lu X-Z., Guo Y., Wang Z-G. *Solid-State Electron*., **49**, 1961 (2005).
5. Page H., Kruck P., Barbieri S., Sirtori C., Stellmacher M., Nagle J. *Electron. Lett*., **35**, 1848 (1999).
6. Page H., Dhillon S., Calligaro M., Becker C., Ortiz V., Sirtori C. *IEEE J. Quantum Electron*., **40**, 665 (2004).
7. Roberts J.S., Green R.P., Wilson L.R., Zibik E.A., Revin D.G., Cockburn J.W., Airey R.J. *Appl. Phys. Lett*., **82**, 4221 (2003).
8. Krysa A.B., Revin D.G., Commin J.P., Atkins C.N., Kennedy K., Qiu Y., Walther T., Cockburn J.W. *IEEE Photon. Technol. Lett.*, **23**, 774 (2011).
9. Sirtori C., Kruck P., Barbieri S., Page H., Nagle J., Beck M., Faist J., Oesterle U. *Appl. Phys. Lett*., **75**, 3911 (1999).
10. Marmalyuk A.A., Ladugin M.A., Andreev A.Yu., Telegin K.Yu., Yarotskaya I.V., Meshkov A.S., Konyaev V.P., Sapozhnikov S.M., Lebedeva E.I., Simakov V.A. *Kvantovaya Elektron.*, **43**, 895 (2013) [*Quantum Electron*., **43**, 895 (2013)].
11. Marmalyuk A.A., Padalitsa A.A., Ladugin M.A., et al. *Ross. Nanotekh.* (in press).
12. Zasavitskii I.I., Pashkeev D.A., Marmalyuk A.A., Ryaboshtan Yu.L., Mikaelyan G.T. *Kvantovaya Elektron*., **40**, 95 (2010) [*Quantum Electron*., **40**, 95 (2010)].
13. Gmachl C., Capasso F., Sivco D.L., Cho A.Y. *Rep. Prog. Phys*., **64**, 1533 (2001).
14. Atkins C.N., Krysa A.B., Revin D.G., Kennedy K., Commin J.P., Cockburn J.W. *Electron. Lett*., **47**, 1193 (2011).